

# Dynamics of bright discrete staggered solitons in photovoltaic photorefractive media

A. Maluckov<sup>1,a</sup>, M. Stepić<sup>2</sup>, D. Kip<sup>2</sup>, and Lj. Hadžievski<sup>3</sup>

<sup>1</sup> Faculty of Sciences and Mathematics, University of Niš, P.O.B. 224, 18001 Niš, Serbia and Montenegro

<sup>2</sup> Institute of Physics and Physical Technologies, Clausthal University of Technology, 38678 Clausthal-Zellerfeld, Germany

<sup>3</sup> Vinča Institute of Nuclear Sciences, P.O.B. 522, 11001 Belgrade, Serbia and Montenegro

Received 22 February 2005

Published online 13 July 2005 – © EDP Sciences, Società Italiana di Fisica, Springer-Verlag 2005

**Abstract.** Theoretical results on spatial optical bright solitons excited in arrays of nonlinear defocusing waveguides, that result from the photovoltaic effect in a photorefractive material, are presented. The existence of four types of stationary discrete bright staggered solitons, on-site, inter-site, twisted inter-site, and twisted on-site solitons, is shown both analytically and numerically, and their stability properties are investigated. The maximum Hamiltonian of staggered solitons with the same total power corresponds to stable modes. It is shown that for low total power the on-site mode is stable while in the high power regime the inter-site mode is stable. These results are confirmed numerically. In addition, steering properties of localized modes are investigated by introducing a transversal translational shift. Because of the translational symmetry between on-site and inter-site localized modes they are considered as two dynamical realizations of the same moving mode, and the formalism of the Peierls-Nabarro effective potential is applied to interpret the exchange between trapping and steering of these modes. This critically depends on the mode's total power and the introduced phase difference. On the other hand, steering of twisted inter-site and on-site localized modes is not numerically observed. Instead, transversal perturbation leads to a transformation of twisted modes either into a trapped on-site mode of smaller power and radiation, or into two trapped on-site modes.

**PACS.** 42.65.Tg Optical solitons; nonlinear guided waves – 42.82.Et Waveguides, couplers, and arrays – 63.20.Pw Localized modes

## 1 Introduction

The phenomenon of localization through nonlinearity and discreteness has been confirmed by many experimental observations in physical systems ranging from electronic and magnetic solids, through micro-engineered structures including Josephson junctions and optical waveguide arrays, to laser induced photonic crystals [1]. Currently the most interesting experimental and theoretical investigations of these so-called intrinsic localized modes, which are also known as discrete breathers [2,3], are related to Bose-Einstein condensation [4,5], biopolymers [6], and all-optical logic and switching devices [7]. Concerning the last mentioned systems, it has been shown that particularly photorefractive nonlinearities can support self-trapping of optical beams generating diverse types of nonlinear localized modes: quasi-steady-state solitons [8], screening solitons [9], and photovoltaic solitons [10–12]. Experimentally it has been confirmed that spatial solitons resulting from the photovoltaic effect in a photorefractive material differ

from both Kerr and other types of photorefractive solitons in physical origin, dependence on light intensity and material properties, and their temporal behavior [12–14]. For practical purposes interesting properties of photovoltaic solitons are their generation at low (microwatts level and below) power, and complete control of their width through the intensity. Thus the investigation of the characteristics of photovoltaic solitons is a quite intriguing task.

In the present paper one-dimensional (1D) bright discrete photovoltaic solitons are considered both analytically and numerically. The optical pulse propagation in an array of coupled defocusing optical waveguides that are lossless, identical, and regularly spaced is modelled assuming only nearest-neighbor interactions. The theoretical model in form of nonlinear difference-differential equations is presented in Section 2. Note that in the present context, the array of coupled optical waveguides is equivalent of the one-dimensional optical lattice. Two types of stationary solutions are found: homogenous solutions and localized modes, which are discussed in Section 3. Due to the characteristics of self-defocusing media, only staggered localized modes can exist. Among them on-site,

---

<sup>a</sup> e-mail: maluckov@junis.ni.ac.yu

inter-site, twisted inter-site, and twisted on-site bright solitons are distinguished. The existence and stability of these four staggered localized modes are investigated in detail. The propagation of localized modes is governed by two coexisting effects, i.e., spatial diffraction and nonlinearity, and these effects are numerically treated. In addition, the examination of the stability of the obtained localized modes with respect to transversal translational shifts is performed in Section 4. The transversal propagation of the transversally symmetric on-site and inter-site localized modes is considered from the viewpoint of the effective Peierls-Nabarro (PN) potential. A brief overview of the results is presented in the conclusion.

## 2 Model

The evolution equation of optical pulse propagation in the presence of a photovoltaic effect in bulk photorefractive defocusing media can be written as [15]:

$$i \frac{\partial U}{\partial \xi} + \frac{1}{2} \frac{\partial^2 U}{\partial s^2} - \beta \frac{|U|^2 U}{1 + |U|^2} = 0, \quad (1)$$

where  $U = I/I_d$  is the normalized slowly varying envelope of the electric field of the light wave,  $I$  is the intensity of the beam while  $I_d$  is the dark irradiance, and  $\xi = z/kx_0^2$  is a dimensionless coordinate along the beam propagation direction. Here  $x_0$  is an arbitrary spatial width while  $k = 2\pi n_o/\lambda_0$  is the wave number with the unperturbed background refractive index  $n_o$  and light wavelength  $\lambda_0$ . The parameter  $s = x/x_0$  is the normalized transverse coordinate,  $\beta = (kx_0 n_o)^2 r_{33} E_{pv}/2 > 0$  is the nonlinearity parameter,  $r_{33}$  is the electro-optic coefficient, and  $E_{pv}$  is the amplitude of the photovoltaic space charge electric field [12].

We further assume that the evolution of the slowly varying envelopes of the individually guided modes of a homogeneous array of single-mode waveguides can be described by a discrete equation with nearest neighbor interactions of the weakly overlapping fields. For lossless defocusing optical waveguides the normalized model equation derived from (1) then reads:

$$i \frac{\partial U_n}{\partial \xi} + K(U_{n+1} + U_{n-1} - 2U_n) - \beta \frac{|U_n|^2 U_n}{1 + |U_n|^2} = 0, \quad (2)$$

where  $U_n$  is the wave function in the  $n$ th lattice element,  $n = 1, 2, \dots, N$ , with  $U_{N+1} = U_1$  for the case of periodic boundary conditions,  $K = 1/(2h^2)$  is the coupling constant,  $h = (L - Nd)/Nx_0$  is the normalized distance between two elements,  $L$  is the  $x$ -width of the nonlinear waveguide array, and  $d$  represents the width of a single waveguide. In the small amplitude limit  $|U_n|^2 \ll 1$ , equation (2) is the well-known (1+1) discrete nonlinear Schrödinger equation with Kerr nonlinearity [16,17]. In the large amplitude limit the nonlinear term takes the form  $|U_n|^2 U_n / (1 + |U_n|^2) \rightarrow U_n$ .

For an arbitrary value of  $N$ , the system (2) possesses two conserved quantities, total power

$$P = \sum_n |U_n|^2, \quad (3)$$

and Hamiltonian (or the system's total energy)

$$H = \sum_n \{ \beta [|U_n|^2 - \ln(1 + |U_n|^2)] + K |U_{n-1} - U_n|^2 \}. \quad (4)$$

A general analytical solution cannot be obtained since this system is non-integrable. However, a few stationary solutions can be found both numerically and analytically.

In the present paper numerical calculations are performed with the parameter set  $h = 0.5$  and  $\beta = 17.88$ , which corresponds to a distance between two channels of  $4 \mu\text{m}$  and a photovoltaic field of  $E_{pv} = 50 \text{ kV/cm}$ . The model equation is numerically solved by a 6th order Runge-Kutta procedure [18,19] with the stationary solution profile as initial condition. All calculations are performed with double-precision accuracy with regularly checking of the conservation of total power and Hamiltonian. Depending on the solution type and with respect to the periodic boundary conditions, the total number of equations  $N$  is taken as odd or even number (here  $N = 101$  or  $N = 100$ ) which is noted separately in each case.

## 3 Stationary solutions

Among the stationary solutions of our model equation (2), the homogenous solutions (extended modes) and the solutions of solitary type (localized modes) are investigated [12,18,19]. Their existence region and stability properties are considered analytically and numerically in order to understand the localization process governed by diffraction and nonlinearity in the waveguide lattice. It is expected that the transverse propagation of these nonlinear localized modes can be directed by their total power and energy.

### 3.1 Stationary homogenous solutions

The system (2) possesses two trivial homogenous solutions, unstaggered ( $K_b = 0$ ) and staggered ( $K_b = \pi$ ), with lattice-independent constant amplitudes:

$$U_n = U_0 \exp(iK_b n) \exp(i\nu \xi), \quad (5)$$

$$U_{0, \text{unstaggered}} = \sqrt{\frac{\nu}{\beta - \nu}},$$

$$U_{0, \text{staggered}} = \sqrt{\frac{\nu - 4K}{\beta - \nu + 4K}}. \quad (6)$$

The existence range of the unstaggered mode is  $0 < \nu < \beta$ , while the analogous range for the staggered one is  $4K < \nu < \beta - 4K$ . These homogenous solutions have the form of nonlinear Bloch waves as described in the literature [20].

The instability to periodic modulations of a certain wavelength, i.e., modulational instability, is one of the most significant problems related to the propagation of nonlinear homogenous modes [20–23]. The stability properties of homogenous modes are studied by observing the evolution of periodic weak perturbations ( $\propto \cos(2\pi n/N) \exp(i\kappa_b)$ ) [20]. Briefly, a linear stability analysis [19] results in the following dispersion relations:

$$\begin{aligned} \Omega^2 = & 4K^2 \left[ \cos(\kappa_b) \cos\left(\frac{2\pi}{N}\right) - \cos(K_b) \right]^2 \\ & + 4K \left[ \cos(\kappa_b) \cos\left(\frac{2\pi}{N}\right) - \cos(K_b) \right] \\ & \times \left[ 4K \sin^2\left(\frac{K_b}{2}\right) + \frac{(\nu - 4K \sin^2(K_b/2))^2}{\beta} - \nu \right], \end{aligned} \quad (7)$$

where  $\kappa_b = 0$  or  $\kappa_b = \pi$  for unstaggered or staggered perturbations, respectively, and  $\Omega$  determines the time behavior of the perturbation ( $\propto \exp(-i\Omega\xi)$ ). The corresponding instability ranges, which are defined by  $\Omega^2 < 0$  taking into account the existence conditions, are:

$$\nu_2 < \nu_{unst.} < \beta, \quad (8)$$

$$\max(4K, \nu_1) < \nu_{st.} < \min(\nu_2, \beta - \nu + 4K), \quad (9)$$

where

$$\nu_{1,2} = a_2 \frac{1 \pm \sqrt{(1 - 4a_1 a_3 / a_2^2)}}{2a_1}, \quad (\nu_2 > \nu_1) \quad (10)$$

and

$$\begin{aligned} a_1 = & \frac{1}{\beta}, \quad a_2 = 1 + \frac{8K \sin^2(K_b/2)}{\beta}, \\ a_3 = & K \left[ \cos(\kappa_b) \cos\left(\frac{2\pi}{N}\right) - 3 \cos(K_b) + 2 \right] \\ & + \frac{16K^2 \sin^4(K_b/2)}{\beta}. \end{aligned}$$

However, the linear stability analysis gives no information about the behavior of the system when this instability grows. According to earlier results obtained for both Kerr and saturable nonlinearities in a self-defocusing medium [20, 24], it is expected that the process of modulational instability is responsible for energy localization and the creation of discrete solitary solutions.

Our analytical estimations concerning the existence region of both unstaggered and staggered homogenous modes, and the onset of instability are proved numerically. Moreover, the evolution of the system beyond the instability point is checked by additional numerical simulations. The results qualitatively correspond to the case treated in reference [25].

For small power modulational instability results in a concentration of the pulse energy in one waveguide (localization) as plotted in Figure 1a. The pulse profile for higher power is more irregular than for smaller power as is shown in Figure 1b. In accordance with the conclusions

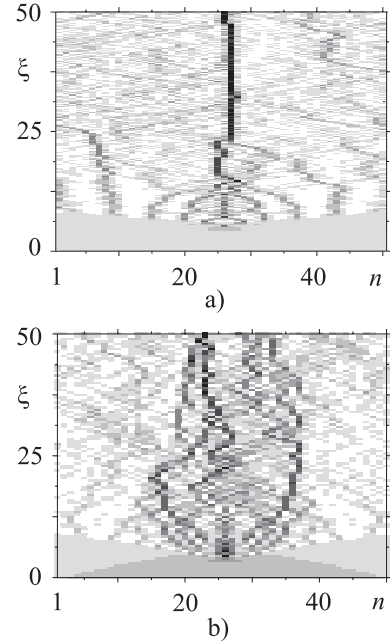


**Fig. 1.** Evolution of an initially modulated staggered homogeneous mode (with added unstaggered periodic perturbation) with total power (a)  $P = 6.3$  and (b)  $P = 22.2$ . The total number of waveguides is  $N = 50$ . In the figure the waveguides are numbered as  $n = 1, 2, \dots, N$ .

derived in [25], the nonlinear mode coupling finally takes over, the number of excited modes increases, and the pulse profile for high power reaches a chaotic-like state in which all wavelengths are present. The transition to this state is sharp and associated with an abrupt rise of the maximum amplitude along the lattice.

### 3.2 Stationary staggered solitary solutions

Stationary localized modes in the form of discrete bright solitons (i.e. nonlinear localized modes with exponentially decaying asymptotics) can be obtained from equation (2) assuming solutions in the form  $U_n(z) = f_n \exp(-i\nu\xi)$  and ordering  $|f_n| \ll |f_{n-1}| \ll \dots \ll |f_{n_c}|$ , where  $n_c$  notes the central waveguide. The resulting set of coupled algebraic equations for the real functions  $f_n$  is:

$$\nu f_n + K(f_{n+1} + f_{n-1} - 2f_n) - \beta \frac{|f_n|^2 f_n}{1 + |f_n|^2} = 0. \quad (11)$$

The two types of stationary localized mode profiles can be distinguished as unstaggered and staggered ones with patterns  $f_n = \exp(iK_b n) F_n$ , where  $K_b = 0$  and  $K_b = \pi$ , respectively, and  $F_n = |f_n| > 0$ . Because of the characteristics of self-defocusing media only staggered localized modes can exist in the actual model. In the corresponding equation that includes reflection symmetry with respect to equation (11) only unstaggered solitary solutions exist.

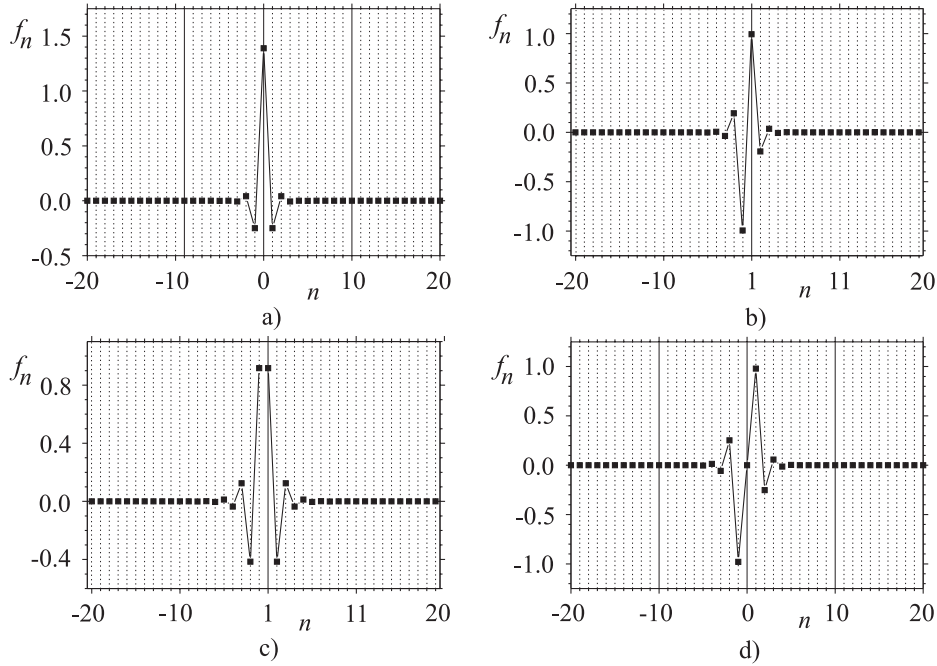


**Fig. 2.** Different staggered localized modes for the same power  $P = 2.056$ : (a) on-site staggered soliton, (b) inter-site staggered soliton, (c) twisted inter-site staggered soliton, and (d) twisted on-site staggered soliton. Note that  $n = \dots -2, -1, 0, 1, 2, \dots$  for on-site and twisted on-site modes, and  $n = \dots -2, -1, 1, 2, \dots$  for inter-site and twisted inter-site localized mode.

### 3.2.1 On-site and inter-site staggered solitons

The two basic types of localized staggered modes are on-site modes that are centered at a nonlinear waveguide element, and inter-site modes centered between two neighboring waveguides (Fig. 2). The waveguide index for on-site modes is  $n = -N/2, -N/2 + 1, \dots, n_c, \dots, N/2 - 1, N/2$ , where  $n_c = 0$  and  $N$  is an odd number, or  $n = -N/2, -N/2 + 1, \dots, -1, 1, \dots, N/2 - 1, N/2$ , where  $n_c = 1$  and  $N$  is an even number for inter-site modes, respectively. Thus,  $f_{|n|} = (-1)^s f_{-|n|-s}$  with  $s = 0$  for on-site modes and  $s = 1$  for inter-site modes [20] ( $|n| = n_c, n_c + 1, \dots, N/2$ ).

When considering on-site staggered localized modes in the lattice elements with  $|n| > 1$ , the total power  $P_o$  and Hamiltonian  $H_o$  can be approximately calculated [19] as:

$$P_o = F_0^2 \frac{(\omega - 2)^2 + 1}{(\omega - 2)^2 - 1}, \quad (12)$$

$$H_o = -\gamma \ln \left( 1 + F_0^2 \right) - 2\gamma \ln \left( \prod_{n=1}^{\infty} \left( 1 + \frac{F_0^2}{(\omega - 2)^{2n}} \right) \right) + 2F_0^2 \frac{\omega - 1}{\omega - 3} + \gamma P_o, \quad (13)$$

where  $\omega = \nu/K$ ,  $\gamma = \beta/K$ , and the amplitude of the on-site staggered soliton is defined as:

$$F_0^2 = \frac{(\omega - 2)^2 - 2}{(\gamma - \omega + 2)(\omega - 2) + 2}, \quad f_{|n|} = f_{-|n|} = (-1)^{|n|} \frac{F_0}{(\omega - 2)^{|n|}}. \quad (14)$$

Adopting the same procedure a inter-site staggered localized mode is characterized by the total power  $P_i$  and Hamiltonian  $H_i$ :

$$P_i = 2F_1^2 \frac{(\omega - 2)^2}{(\omega - 2)^2 - 1}, \quad (15)$$

$$H_i = -2\gamma \ln \left( \prod_{n=1}^{\infty} \left( 1 + \frac{F_1^2}{(\omega - 2)^{2(n-1)}} \right) \right) + 2F_1^2 \frac{3\omega - 7}{\omega - 3} + \gamma P_i. \quad (16)$$

Here the corresponding amplitudes of inter-site staggered modes in each waveguide can be written as:

$$F_1^2 = \frac{(\omega - 3)(\omega - 2) - 1}{(\gamma - \omega + 3)(\omega - 2) + 1}, \quad f_{|n|} = -f_{-|n|} = (-1)^{|n|-1} \frac{F_1}{(\omega - 2)^{|n|-1}}. \quad (17)$$

### 3.2.2 Twisted on-site and inter-site staggered solitons

It has been shown in the literature that, because of a periodic modulation of the medium's refractive index, two out-of-phase bright solitons can form bound states, so-called 'twisted' localized modes [20, 26]. Such solutions do not have their continuous counterparts, and they exist only when the discreteness effects are strong (for fixed value  $\beta = 17.88$ ,  $h > 0.4$ ). The properties of these twisted modes depend on the separation between the modes forming a bound state. Here the existence of staggered twisted modes is shown analytically and numerically.

Following the procedure developed for on-site and inter-site staggered localized modes total power  $P$ , Hamiltonian  $H$ , and amplitude of the inter-site twisted staggered mode (with the pattern  $\dots, f_{-2} = -F_2, f_{-1} = F_1, f_1 = F_1, f_2 = -F_2, \dots$  where  $F_n$  is always a positive number, Fig. 2c) are approximately:

$$P_{ti} = 2F_1^2 \frac{(\omega - 2)^2}{(\omega - 2)^2 - 1} \quad (18)$$

$$H_{ti} = -2\gamma \ln \left( \prod_{n=1}^{\infty} \left( 1 + \frac{F_1^2}{(\omega - 2)^{2(n-1)}} \right) \right) + 2F_1^2 \frac{\omega - 1}{\omega - 3} + \gamma P_{ti} \quad (19)$$

$$F_1^2 = \frac{(\omega - 3)(\omega - 1) - 1}{(\gamma - \omega + 1)(\omega - 2) + 1},$$

$$f_{|n|} = f_{-|n|} = (-1)^{|n|-1} \frac{F_1}{(\omega - 2)^{|n|-1}}. \quad (20)$$

In addition, the model equation (2) allows one more type of stationary staggered photovoltaic solitons, the so-called twisted on-site staggered localized mode with a pattern in the form  $\dots, f_{-2} = F_2, f_{-1} = -F_1, f_0 = 0, f_1 = F_1, f_2 = -F_2, \dots$  Figure 2d. The total power, Hamiltonian, and amplitudes at the waveguide sites can be written as:

$$P_{to} = F_1^2 \frac{(\omega - 2)^2}{(\omega - 2)^2 - 1} \quad (21)$$

$$H_{to} = -2\gamma \ln \left( \prod_{n=1}^{\infty} \left( 1 + \frac{F_1^2}{(\omega - 2)^{2(n-1)}} \right) \right) + 4F_1^2 \frac{\omega - 2}{\omega - 3} + \gamma P_{to} \quad (22)$$

$$F_1^2 = \frac{(\omega - 3)(\omega - 1)}{(\gamma - \omega + 2)(\omega - 2) + 1},$$

$$f_{|n| \geq 1} = -f_{-|n|} = (-1)^{|n|-1} \frac{F_1}{(\omega - 2)^{|n|-1}}. \quad (23)$$

The relations  $H(P)$  for all localized modes obtained analytically using equations (12–23) can fairly well reproduce the corresponding numerically observed curves. The numerically obtained shapes of curves  $H(P)$  for all localized staggered modes are presented in Figure 3. In addition, the existence region of stationary staggered solitons estimated analytically (Eqs. (12–23)) and numerically is approximately:  $4 < \omega < \gamma + 4$ .

### 3.2.3 Stability of the staggered localized modes

Considering the stability of staggered localized modes it is worth to mention that the compensation of discrete diffraction and nonlinearity, which results in the formation of localized staggered modes, is here possible only by relating a negative effective mass to the system [5,16]. Then the sign of diffraction is reversed when compared with the problem with reflection symmetry, where the un-staggered mode with minimum Hamiltonian is stable. This

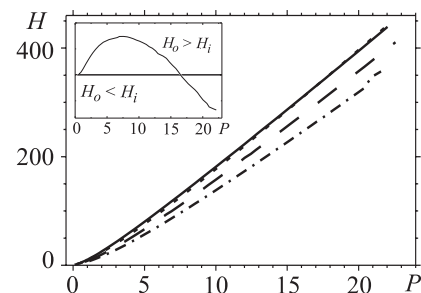


**Fig. 3.** Hamiltonian  $H$  versus total power  $P$  for on-site (solid curve), inter-site (dashed curve - short dashes), twisted inter-site (dash-dotted curve), and twisted on-site (dashed curve - long dashes) solitons. The inset shows the difference of Hamiltonians for on-site ( $H_o$ ) and inter-site soliton ( $H_i$ ).

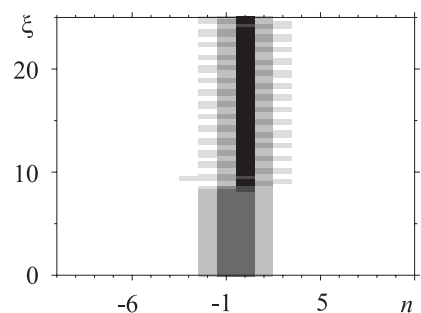


**Fig. 4.** Conversion of an inter-site mode of small power  $P = 2.056$  into the corresponding on-site mode with the same power for  $H_i < H_o$ . Note that  $n = \dots, -2, -1, 1, 2, \dots$

results in the stability of the staggered mode with maximum Hamiltonian. Our numerical calculations confirm this stable propagation of an on-site staggered localized mode with  $P < 16$  when  $H_{max} = H_o$ , or an inter-site localized mode with  $P < 0.5$  when  $H_{max} = H_o \approx H_i$  and  $P > 16$  when  $H_{max} = H_i$ , as can be seen in Figure 3. The inter-site staggered mode converts into an on-site staggered mode with the same power for power ranges with  $H_{max} = H_o$  (Fig. 4), and an on-site staggered mode converts into an inter-site staggered mode with equal power when  $H_{max} = H_i$ . As can be seen, the regions of small power on-site and inter-site modes,  $P < 0.5$ , and higher power on-site and inter-site modes with  $P \approx 16$ , are characterized by simultaneous stability of both mentioned modes. It happens if  $H_o \approx H_i$  and is signed as the marginal stability region. As expected, the stability properties of the localized on-site and inter-site solitons for small values of  $P$  are in accordance with the corresponding behavior of systems with defocusing Kerr nonlinearity [19].

Alternatively, the stability of the localized modes is considered in the context of the convexity of the Hamiltonian vs. total power curve [27]. According to the analysis in [27], the convexity of the  $H - P$  curve ( $d^2H/dP^2 > 0$ ) is the necessary condition for the stability of the localized mode in the self-defocusing media. In our case all coexisting localized modes satisfy the condition  $d^2H/dP^2 > 0$  (Fig. 3) and for the given value of total power  $P$  the

stable one is the localized mode with the maximum value of the Hamiltonian.

Considering the inter-site twisted and on-site twisted solitons, the numerical analysis reveals that both types are always unstable with respect to transversal perturbations. This behavior can be associated with the ordering of the values of the corresponding Hamiltonians for localized modes plotted in Figure 3. Namely, for a given power the value of the Hamiltonian for both twisted modes is smaller than the corresponding values for on-site and inter-site localized modes.

#### 4 Steering effect

In this section the dynamics of propagating localized modes is considered. The translational symmetry between on-site and inter-site staggered solitons allows to consider them as two dynamical states of a single moving mode [28]. Then the concept of the PN effective potential [2, 19, 29, 28] caused by the system's discreteness can be applied for interpretation of their dynamical properties. The amplitude of the PN potential is considered equal to the minimum barrier which must be overcome to translate the center of mass of the system by half a lattice period. Correspondingly, the PN potential is the difference in energy between on-site and inter-site stationary localized modes for the same power level  $P_o = P_i = P$ :

$$\Delta E_{oi} = H_o - H_i. \quad (24)$$

In Figure 5 the shape of the curve  $\Delta E_{oi}(P)$  generated numerically is presented. As can be seen,  $\Delta E_{oi}(P)$  is positive for small and mediate  $P$  values and becomes negative for high  $P > 16$ . The curve  $\Delta E_{oi}(P)$  obtained analytically using equations (12–23) can be fairly well fitted to the corresponding numerically obtained curve, especially in the region of low and mediate power, as shown in Figure 5.

Finally, it is worth to mention a particularity of the present type of nonlinearity (Eq. (2)) when observing the amplitudes in the central waveguide and two first neighbors, Figure 6. Here the amplitudes in the central waveguides monotonically increase changing only the increasing rate with total power from small values for small and medium powers to the very high increasing rate for high powers. Note that in the last limit the nonlinearity reduces to the linear term (see Sect. 2). This is different from the cascade nature of the amplitude saturation in reference [18] and related with the shape of the PN potential. Accordingly, in present case the PN potential do not possess several zeros as in reference [19].

The localized modes are numerically forced to move transversally by introducing a small phase difference (phase offset) between adjacent lattice elements [21] in the form  $\exp(ikn)$ , where the parameter  $k$  is noted as the phase difference. An input on-site or inter-site soliton with small total power ( $P < 0.5$ ) and small PN potential (Fig. 5) having a linear phase gradient can excite moving breathers, which propagate under small angles relative to the waveguide channels. The steering velocity is

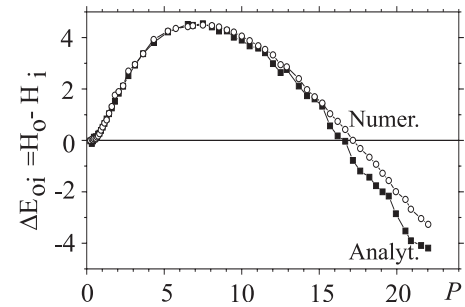


**Fig. 5.** Comparison of analytically and numerically obtained PN effective potential,  $\Delta E_{oi} = H_o - H_i$ , versus soliton power  $P$ .

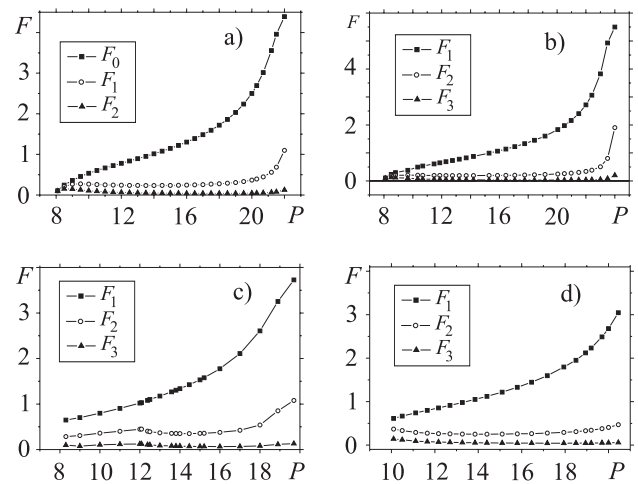


**Fig. 6.** Absolute value of amplitudes  $F_n = |f_n|$  in the central waveguide and the first two neighbors as a function of  $P$  for (a) on-site, (b) inter-site, (c) twisted inter-site, and (d) twisted on-site stationary solitons.

proportional to the introduced phase difference, which is illustrated in Figure 7. As the PN potential increases, the direction of transversal propagation may change and finally, when the soliton cannot overcome the PN potential, the inter-site and on-site mode transform into a trapped on-site breather in one of the waveguide channels. An example is given in Figure 8. Trapping prevails also in the region of the second zero of the PN potential where highly localized modes (i.e. modes with high power) are very robust and may resist transversal shifts. Above the last mentioned PN potential value, i.e. in the region with negative PN potential, the phase tilted localized mode converts into a trapped inter-site breather.

The dynamics of twisted inter-site and twisted on-site solitons with phase offsets is rather complex. The twisted inter-site and twisted on-site modes are transformed into a trapped on-site breather with either the same (this appears only for twisted inter-site modes with small powers  $P < 7$  and small phase tilt) or smaller total power. In the latter case, the difference in the corresponding power leads to energy radiation into the lattice. On the other hand, twisted inter-site modes with higher power as well as twisted on-site modes can be converted by an

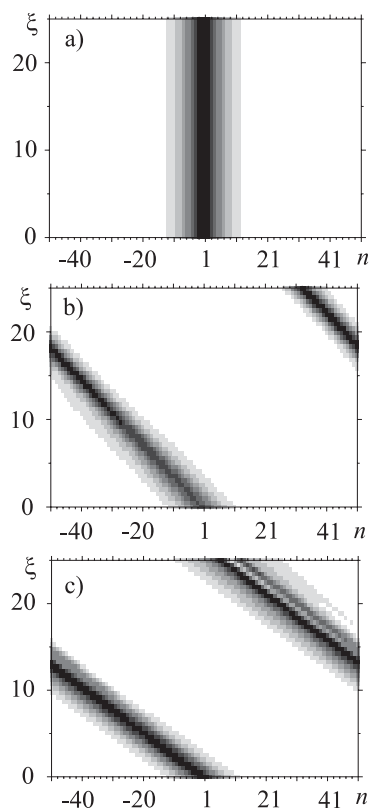


**Fig. 7.** Steering of an inter-site localized mode with  $P = 0.1$  as a function of relative phase difference  $k$ : (a)  $k = 0$  (stable propagation), (b)  $k = 0.25\pi$  (moving breather), and (c)  $k = 0.5\pi$  (moving breather that is faster than in (b)). Note that  $n = \dots, -2, -1, 1, 2, \dots$

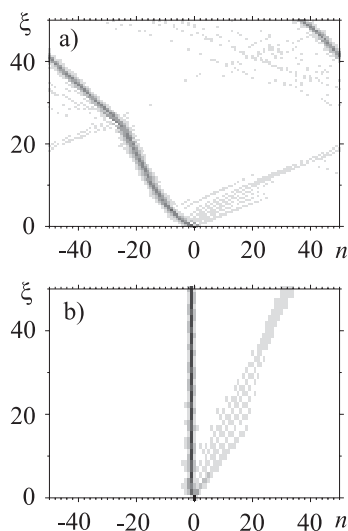


**Fig. 8.** Steering effect of on-site modes with (a)  $P = 0.582$ ,  $k = 0.5\pi$  (free movement) and (b)  $P = 0.655$ ,  $k = 0.5\pi$  (trapping).

appropriate phase tilt into two trapped breathers with smaller total power, as illustrated in Figure 9, in consistency with the conservation of both  $P$  and  $H$ .

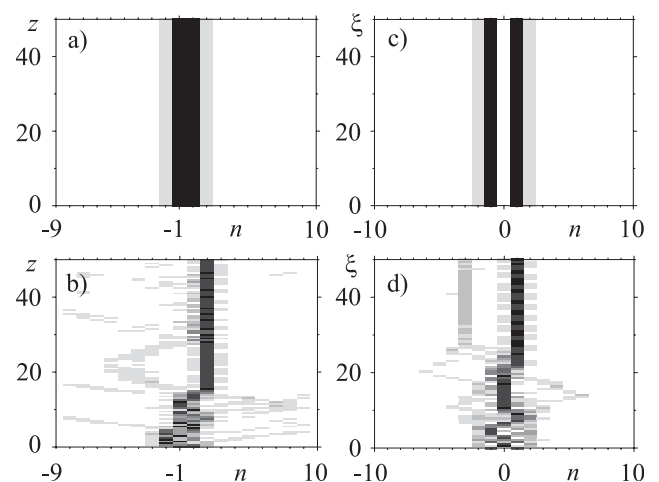


**Fig. 9.** Twisted inter-site mode with  $P = 9.265$  (a) without relative phase difference,  $k = 0$ , and (b) with  $k = 0.25\pi$ . In the latter case the twisted mode converts into an on-site mode and radiation. In addition the evolution of twisted on-site localized modes with  $P = 12.693$  is shown: (c) without mode distortion for  $k = 0$  and (d) with resulting conversion into two localized modes for  $k = 0.5\pi$ .

## 5 Conclusion

In conclusion, we have done a step ahead in understanding the nature and behavior of internal localized modes governed by both discreteness and nonlinearity, which is an important issue in the context of many diverse fields such as dynamical lattices, repulsive Bose-Einstein condensates in periodic potentials, solid state physics, nonlinear optics, etc. The propagation of bright spatial discrete solitons that results from the photovoltaic effect in a photorefractive material is modelled. It has been shown that self-focusing may be observed in an array of coupled defocusing nonlinear waveguides and that this effect leads to the creation of self-localized, soliton-like patterns with characteristic relative phase differences of  $\pi$  between neighboring waveguides, named staggered localized modes. Four localized patterns are found analytically: on-site, inter-site, twisted inter-site, and twisted on-site staggered modes, and their existence is confirmed numerically. The stability of the staggered localized mode with the maximum Hamiltonian is numerically confirmed. It is shown that two stability regions exist: in the small power region on-site modes are stable while in the high power region inter-site modes are stable.

The transversal propagation, i.e. steering of the on-site and inter-site modes as two dynamical states of the same localized mode, are considered in the context of the Peierls-Nabarro potential barrier. Our numerical results demonstrate the mobility of on-site and inter-site staggered localized modes in the low power region with low PN barrier. Increasing the power and thus the PN barrier leads to decreasing of soliton mobility eventually followed by spatial trapping of the modes on a lattice site. The enhanced mobility of high power solitons near the zero of the PN barrier is not observed numerically. On the other hand,

steering of twisted inter-site and on-site localized modes is not numerically observed, too. Instead, transversal perturbation leads to a transformation of twisted modes either into a trapped on-site mode with smaller power and radiation, or into two trapped on-site modes.

This work is carried out under the auspices of the Ministry of Science, Development and Technologies of Republic Serbia (project 1964) and the German Federal Ministry of Education and Research (BMBF, grant DIP-E6.1).

## References

1. D.K. Campbell, S. Flach, Yu.S. Kivshar, *Phys. Today* **57**, 43 (2004)
2. P.J. Martinez et al., *Chaos* **13**, 610 (2003)
3. G.P. Tsironis, *Chaos* **13**, 657 (2003)
4. J.C. Bronski et al., *Phys. Rev. E* **63**, 036612 (2001)
5. V. Ahufinger et al., *Phys. Rev. A* **69**, 053604 (2004)
6. J.C. Eilbeck, P.S. Lomdahl, A.C. Scott, *Physica D* **16**, 318 (1985)
7. D.N. Christodoulides, E.D. Eugenieva, *Phys. Rev. Lett.* **87**, 233901 (2001)
8. D.N. Christodoulides, M.I. Carvalho, *Opt. Lett.* **19**, 1714 (1994)
9. G. Couton, H. Maillotte, M. Chauvet, *J. Opt. B: Quantum Semiclass. Opt.* **6**, 5223 (2004)
10. G.C. Valley et al., *Phys. Rev. A* **50**, R4457 (1994)
11. M. Chauvet, *J. Opt. Soc. Am. B* **20** (12), 2515 (2003)
12. M. Segev et al., *J. Opt. Soc. Am. B* **14**, 1772 (1997)
13. D.N. Christodoulides, R.I. Joseph, *Opt. Lett.* **13**, 794 (1988)
14. H. Eisenberg et al., *Phys. Rev. Lett.* **81**, 3383 (1998)
15. Yu. S. Kivshar, V.V. Afanasjev, *Opt. Lett.* **21**, 1137 (1996)
16. D. Cai, A.R. Bishop, N. Grønbech-Jensen, *Phys. Rev. Lett.* **72**, 591 (1994)
17. H. Feddersen, in *Nonlinear Coherent Structures in Physics and Biology*, Lecture Notes in Physics, Vol. 393 (Springer-Verlag, Berlin, 1991), p. 159
18. M. Stepić et al., *Phys. Rev. E* **69**, 066618 (2004)
19. Lj. Hadžievski et al., *Phys. Rev. Lett.* **93**, 033901 (2004)
20. A.A. Sukhorukov et al., *IEEE J. Quantum Electron.* **39**, 31 (2003)
21. Yu. S. Kivshar, D.E. Pelinovsky, *Phys. Rep.* **331**, 117 (2000)
22. S. Darmanyan, I. Relke, F. Lederer, *Phys. Rev. E* **55**, 7662 (1997)
23. J. Meier et al., *Phys. Rev. Lett.* **92**, 163902 (2004)
24. Yu. S. Kivshar et al., *Phys. Rev. B* **58**, 5423 (1998)
25. Yu. S. Kivshar, M. Peyrard, *Phys. Rev. A* **46**, 3198 (1992)
26. P.G. Kevrekidis, A.R. Bishop, K.Ø. Rasmussen, *Phys. Rev. E* **63**, 036603 (2001)
27. N. Akhmediev, A. Ankiewicz, *Phys. Rev. E* **59**, 6088 (1999)
28. Yu. S. Kivshar, D.K. Campbell, *Phys. Rev. E* **48**, 3077 (1993)
29. Ch. Claude et al., *Phys. Rev. B* **47**, 14228 (1993)